

Quantum displacement sensing and cooling in 3D levitated cavity optomechanics

M. Toroš¹ and T.S. Monteiro^{1,*}

¹*Department of Physics and Astronomy, University College London,
Gower Street, London WC1E 6BT, United Kingdom*

Ultra-high sensitivity detection of quantum-scale displacements in cavity optomechanics optimises the combined errors from measurement back-action and imprecisions from incoming quantum noises. This sets the well-known Standard Quantum Limit (SQL). Normal quantum cavity optomechanics allows cooling and detection of a single degree of freedom, along the cavity axis. However, a recent breakthrough that allows quantum ground-state cooling of levitated nanoparticles [Delic et al, arXiv:1911.04406], is uniquely 3D in character, with coupling along the x , y and z axes. We investigate current experiments and show that the underlying behaviour is far from the addition of independent 1D components and that ground-state cooling and sensing analysis must consider- to date neglected- 3D hybridisation effects. We characterise the additional 3D spectral contributions and find direct and indirect hybridising pathways can destructively interfere suppressing of 3D effects at certain parameters in order to approach, and possibly surpass, the SQL. We identify a sympathetic cooling mechanism that can enhance cooling of weaker coupled modes, arising from optomechanically induced correlations.

The coupling of mechanical motion to the optical mode of a cavity permits not only strong cooling but also ultra-sensitive displacement detection, and has led to advances ranging from quantum ground state cooling of mechanical oscillators [1, 2] to detection of gravitational waves by LIGO [3]. Optomechanics employing levitated dielectric particles has recently also experienced rapid development [4, 5]. The unique potential of levitated cavity optomechanics in terms of decoupling from environmental heating and decoherence, coupled with the sensitivity of displacement sensing offered by optical cavities was already recognised in 2010 [6–8]. Actual experimental realisations represent a formidable technical challenge: the levitated nanoparticle must be cooled from room temperatures, and is initially millions of quanta above the quantum ground state.

Most initial proposals were for self-trapping set-ups [7, 9, 10], with trapping and cooling both provided by the cavity modes [11], but this failed to allow stable trapping at high vacuum [10–12]. In order to overcome this road-block, hybrid set-ups combining for instance a tweezer and cavity traps [6, 13]; or a hybrid electro-optical trap [14, 15], or a tweezer and near-field of a photonic crystal [16], allowed some progress towards the ultimate goal of quantum ground state cooling.

This year, an important breakthrough was the realisation that the tweezer trapping light coherently scattered (CS) into an undriven cavity offers major advantages [17–19]: the resulting optomechanical couplings along every axis can be comparatively large even for modest mean cavity photon numbers, minimising the deleterious effects of photon scattering [20–22]. As a result, quantum cooling of the centre of mass of a levitated nanoparticle to phonon occupancies $n_x < 1$ along the x axis (see Fig.1

for definition of axes)) was recently reported [23].

Here we investigate the 3D cooling and displacement sensing for CS systems. We obtain expressions for 3D spectra that reproduce experimental features, and yield excellent agreement with stochastic numerics using the tweezer and cavity potentials without linearisation. We consider direct intermode couplings overlooked previously and find they introduce interference pathways that can (tunably) cancel hybridisation between modes, without which the spectra and SQL analysis cannot in general be understood. While multi-mechanical-mode set-ups are not unusual in cavity optomechanics, typically those modes have widely differing quality factors or effective masses. In contrast, the fully equivalent and strongly cooled modes here offer a new and unparalleled range of hybridisation and mutual back-action effects. In the experimental regimes of [23], we find that a strongly-cooled x mode is cooled to phonon occupancy $n_x \sim 1$, but conclude that inclusion of hybridisation effects is essential for reliable thermometry. Separately, a weakly-coupled y mode experiences sympathetic cooling mechanism that lowers n_y significantly, due to optomechanical correlations, analogous to the ponderomotive squeezing mechanism, but between *mechanical* modes.

Displacement sensing. — For a cavity mode \hat{a} , displacement sensing will involve a measurement of some quadrature of the optical field $\hat{Q}^\Phi = e^{-i\Phi}\hat{a} + e^{i\Phi}\hat{a}^\dagger$, with coupling to a mechanical displacement \hat{q} , usually set by the cavity axis, with coupling strength g described by the well known equation of linearised optomechanics:

$$\hat{Q}^\Phi(\omega) = ig\eta^{(\Phi)}\hat{q}(\omega) + \sqrt{\kappa}\tilde{Q}_{\text{in}}^\Phi, \quad (1)$$

where $\tilde{Q}_{\text{in}}^\Phi$ represent measurement imprecision, typically from incoming quantum photon shot-noise, while κ is the cavity linewidth. $\eta^{(\Phi)} \equiv \eta^{(\Phi)}(\omega)$ is the optical susceptibility, describing the spectral shape of the cavity resonance. Understanding the Standard Quantum Limit

* t.monteiro@ucl.ac.uk

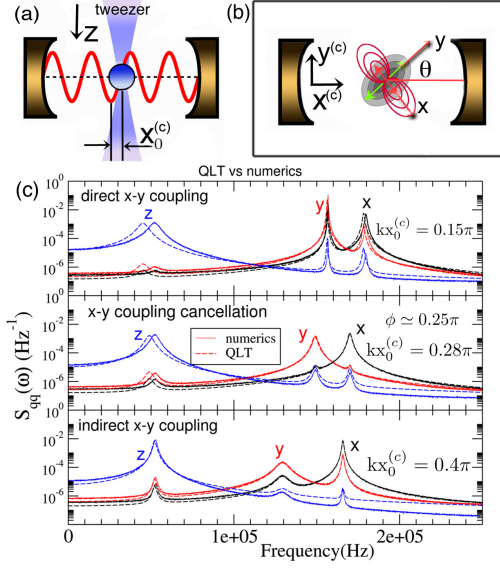


FIG. 1. (a) Schematic of 3D cooling set-up in levitated optomechanics: a nanoparticle held by a tweezer trap within a cavity. The cavity is undriven, but is populated by photons coherently scattered from the tweezer. The nanoparticle is placed at a point $\phi \simeq kx_0^{(c)}$ from the anti-node of the cavity field. Cooling and detection of the centre of mass displacement in 3D along x, y, z is possible. (b) The pattern of coherent photon scattering (taken from [21]) into the cavity depends on the tilt θ of the tweezer polarization axis. (c) Compares displacement PSDs using analytical expressions for the 3D theory (dashed lines) with stochastic numerics using the tweezer and cavity potentials (solid lines). The latter does not assume any values for the optomechanical coupling strengths or equilibrium positions, and includes nonlinearities. x (black), y (red) and z (blue). Agreement between analytics and numerics is excellent. The high degree of hybridisation of x, y modes results in a prominent double-peaked structure (even for $\Delta \gg \omega_k$) for (i) low ϕ (top panel), because of direct coupling g_{xy} and (ii) large $\phi \sim 0.4\pi$ (bottom panel) because of indirect cavity mediated coupling $g_x g_y$. In contrast, *suppression of hybridisation* is seen at $\phi \approx \pi/4$ (middle panel), where destructive interference between the direct and indirect pathways decouples the modes. Parameters in (a) similar to the experiment in [21]: input power $P_{\text{in}} = 0.17\text{W}$, $\Delta = -300$ kHz; however sphere radius $R_0 = 100\text{nm}$ and finesse $\mathcal{F} = 150,000$ are slightly larger, with gas pressure $P = 10^{-6}$ mbar, and $\theta = 0.2\pi$.

(SQL) of displacement sensing in optomechanics usually proceeds via analysis of errors in Eq. (1) or related forms.

In 3D, the measured optical quadrature in general couples to displacements \hat{q}_j along all directions $j = x, y, z$:

$$\hat{Q}^\Phi(\omega) = i \sum_j g_j \eta^{(\Phi_j)} \hat{q}_j(\omega) + \sqrt{\kappa} \tilde{Q}_{\text{in}}^\Phi, \quad (2)$$

where $\Phi_j \equiv \Phi$ for the normal optomechanical case where displacement couples to the amplitude of the light, but $\Phi_j \equiv \Phi - \pi/2$ for the new scenario in the CS experiments [20–22] where it can couple to the optical phase quadra-

ture. Above, $\eta^{(\Phi)} = e^{-i\Phi} \chi(\omega, -\Delta, \kappa) - e^{i\Phi} \chi^*(-\omega, -\Delta, \kappa)$ where $\chi(\omega, -\Delta, \kappa) = [-i(\omega + \Delta) + \frac{\kappa}{2}]^{-1}$ and Δ is the detuning of the light from the cavity resonance.

In the well-known quantum linear theory (QLT) of cavity optomechanics [1, 2], the 1D case is straightforward: the displacement spectra are calculated from cavity amplified noise fluctuations $\tilde{\mathcal{D}}_j^{1D}$, comprising thermal fluctuations of the mechanical modes in addition to the fluctuations representing the back-action effect of the incoming photon shot-noise. Neglecting certain normalisation terms (see [24] for full-details) we have:

$$\hat{q}_j(\omega) \equiv \tilde{\mathcal{D}}_j^{1D} \simeq \sqrt{\Gamma} \tilde{Q}_j^{\text{therm}}(\omega) + i\sqrt{\kappa} g_j \mu_j(\omega) \tilde{Q}_{\text{in}}^{(\Phi=0)} \quad (3)$$

where Γ is a mechanical damping, and $\mu_j(\omega) = \chi(\omega, \omega_j, \Gamma) - \chi^*(-\omega, \omega_j, \Gamma)$ is a mechanical susceptibility function that determines the back-action spectrum generated by incoming quantum shot noise $\tilde{Q}_{\text{in}}^{(\Phi=0)}(\omega)$. In the above 1D equations, the $\tilde{Q}_j^{\text{therm}}(\omega)$ might represent the true signal we wish to measure, while the imprecision and measurement back-action contributions in Eqs. (1) and (3) represent measurement errors: minimising their combined effect yields the well-known SQL [1, 2].

With a simple adjustment to relate the intracavity field to the cavity output field via input-output relations, the corresponding PSD of the measured signal is used to estimate a displacement spectrum $S_{\hat{Q}^\Phi \hat{Q}^\Phi} \simeq g^2 |\eta^{(\Phi)}|^2 S_{qq}^{1D}$ in the 1D case. A key question is whether one might straightforwardly extend to the 3D displacement spectra by simply considering the sum of the independent PSD contributions $S_{\hat{Q}^\Phi \hat{Q}^\Phi} \simeq \sum_{j=x,y,z} g_j^2 |\eta^{(\Phi_j)}|^2 S_{q_j q_j}^{1D}$. We show below that this is not the case.

3D Cavity optomechanics.— As a first approximation to a 3D system, one might simply replace, in Eq. (2), $\hat{q}_j(\omega) \rightarrow \tilde{\mathcal{D}}_j^{1D}$ and directly obtain the PSD for the homodyne spectrum, in other words replace the displacement noises by their 1D equivalents. We note that even in this straightforward case, the error analysis does not simply yield a sum of the 1D PSDs $S_{q_j q_j}^{1D}$: while the thermal contributions are uncorrelated and thus contribute independently to the PSDs, the separate back-actions are all correlated with each other and with the imprecision noises. This is important: even in the 1D case, correlations between back-action and imprecision underlie well-known observed quantum spectral signatures such as sideband asymmetries and optical (ponderomotive) squeezing. Correlations between optical back action and imprecision noise also play an important role in LIGO displacement sensing [25].

Our key findings is that we find additional, genuinely 3D, contributions and we can write the displacement noise spectrum in the form:

$$\hat{q}_j(\omega) \simeq \tilde{\mathcal{D}}_j^{1D} + \sum_{k \neq j} \mathcal{G}_{jk}^{3D}(\omega) \tilde{\mathcal{D}}_k^{1D} \quad (4)$$

from which we can obtain all PSDs analytically. Specifically, each displacement, in addition to the usual 1D

noises terms, receives contributions from the 1D noises of the other two degrees of freedom, determined by a 3D coupling function $\mathcal{G}_{jk}^{3D}(\omega)$ which we can give in closed form and which quantifies the deviation from 1D behaviour (numerical precision includes higher order correction terms, see [24], though for clarity we discuss only the lowest order here).

To understand $\mathcal{G}_{jk}^{3D}(\omega)$, we revisit the quadratic forms of the Hamiltonians of linearised optomechanics, obtained by considering small displacements from an equilibrium point $(x_0, y_0, z_0, \bar{\alpha})$ where the mean photon number in the cavity is $n_p = |\bar{\alpha}|^2$. Usually one writes $\hat{H}/\hbar = \hat{h}^{(0)} + \sum_j \hat{h}_j^{(\text{int})}$ where $\hat{h}^{(0)} = -\Delta \hat{a}^\dagger \hat{a} + \sum_j \omega_j \hat{b}_j^\dagger \hat{b}_j$, $\hat{h}_j^{(\text{int})} = g_j(\hat{a}^\dagger + \hat{a})\hat{q}_j$, $\hat{q}_j = \hat{b}_j^\dagger + \hat{b}_j$, and we have $\Delta < 0$ for a red-detuned cavity.

However, the full Hamiltonian to quadratic order should be $\hat{H}/\hbar = \hat{h}^{(0)} + \sum_j \hat{h}_j^{(\text{int})} + \sum_{j < k} g_{jk} \hat{q}_j \hat{q}_k$ where the last term on the right-hand side contains (previously neglected) direct coupling terms of strength g_{jk} . These are distinct from nonlinear, position squared coupling terms $g_j(\hat{a}^\dagger + \hat{a})\hat{q}_j^2$ which lead to observed sidebands at $2\omega_j$ in optically trapped systems at higher temperatures [15, 21].

In particular, starting from the Hamiltonian including g_{jk} couplings, where we have assumed the usual amplitude quadrature coupling, we obtain:

$$\mathcal{G}_{jk}^{3D}(\omega) = \frac{i\mu_j(\omega)}{M_j(\omega)} \left[i\eta^{(0)}(\omega)g_jg_k + g_{jk} \right]. \quad (5)$$

The prefactor, where $\mu_j(\omega)$ is the mechanical susceptibility and $M_j = 1 + g_j^2 \mu_j \eta^{(0)}$ is a function peaked around one of the mechanical frequencies, i.e. $\omega \approx \pm\omega_j$. However, it is the terms in the square brackets that are of most interest. One can see they describe the interference between a direct, $\propto g_{jk}$, and a cavity mediated, indirect coupling, $\propto g_jg_k$, between any two displacements. In other words, suppressing or conversely, enhancing 3D dynamics will involve either suppressing or correspondingly enhancing the 3D coupling via destructive or constructive interference of direct and indirect pathways near $\omega \approx \omega_j$.

Tweezer-cavity setup.— The above is quite generic to an arbitrary 3D optomechanics set-up. Here we apply this to the new experiments pioneered in [20, 21] which involve levitating a dielectric nanoparticle in a tweezer within a cavity. The tweezer polarization and the cavity axis are tilted at an angle θ (see Figs. 1(a) and 1(b)). The cavity in these set-ups is undriven but is populated entirely by light coherently scattered from the tweezer field and the particle moves under the combined effect of the tweezer trapping field and the coherently scattered light as explained in [20, 21]. We give the full potential in [24], but to a good approximation, the tweezer represents a trapping Hamiltonian equivalent to $\hat{h}^{(0)}$, while

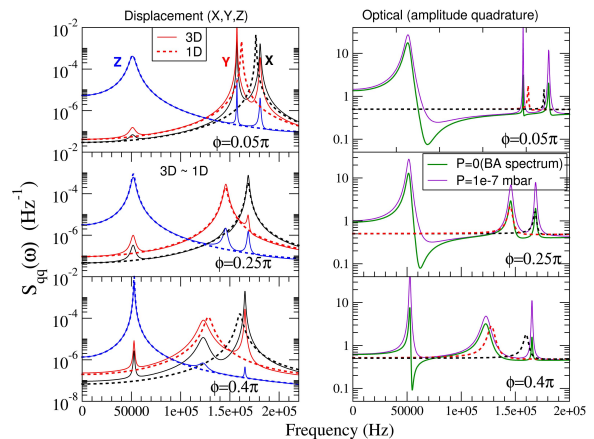


FIG. 2. **(a)** Comparison between full 3D QLT (solid lines) with the equivalent 1D QLT (dotted lines) for the PSDs of the x , y , and z displacements (denoted by black, red, and blue colors, respectively). While 3D QLT includes all optomechanical couplings g_x, g_y, g_z and g_{xy}, g_{xz}, g_{yz} for the full coupled problem, 1D QLT obtains three independent PSDs $S_{q_j}^{1D}$ with all couplings set to zero except g_j . Parameters are similar to Fig. 1, with $-\Delta \gg \omega_j$, but pressure is set to $P = 10^{-7}$ mbar for phonon occupancies near the quantum regime $n \sim 1 - 3$. While in general the x and y 3D PSDs are strongly perturbed (have a double-peaked structure) we see that for $\phi \simeq \pi/4$ (middle panels) they are very close to their 1D forms as there is destructive interference between direct and indirect pathways. The z mode contributes only weakly as it is well separated in frequency. At lower (higher) ϕ there are large differences between 1D and 3D PSDs due to the direct (indirect) pathways as seen in the top (bottom) panels. **(b)** For the optical output spectra (corresponding to homodyne detection of the amplitude quadrature of the cavity output, violet lines) the very large squeezing by the z mode at $\phi \sim 0$ lowers the imprecision floor for the x and y PSDs. For comparison we plot also the measurement back-action (BA) spectra (green curves) obtained for $P \rightarrow 0$. Dotted lines are the 1D BA equivalent and once again, at $\phi = \pi/4$ these are also very close to the 3D form.

the interaction with the cavity mode yields the potential:

$$\frac{\hat{V}_{\text{int}}}{\hbar} = -E_d \cos[\phi + k(\hat{x} \sin \theta + \hat{y} \cos \theta)] \hat{a} e^{-i\beta(z)} + \text{H.c.} \quad (6)$$

where $\phi \sim kx_0^{(c)}$, $x_0^{(c)}$ is the displacement between the tweezer focus and an antinode of the cavity (see Fig. 1(a)), $\beta(z) = kz - \arctan(z/z_R)$, z_R is the Rayleigh range, and E_d is the coupling rate determined by the particle polarisability and input power to the tweezer. Expanding \hat{V}_{int} to quadratic order provides the light-matter couplings g_j , the matter-matter couplings g_{kj} as well as corrections to the mechanical frequencies and the equilibrium points (see [24] for details).

The direct coupling has not previously been considered in the experimental analysis [20–22] but we find they can be of great importance; one can show that

$g_{xy} \simeq -g_x g_y \frac{2\text{Re}(\bar{\alpha}) \cos \phi}{E_d \sin^2 \phi}$, while $g_{jz} \simeq g_j g_z \frac{2\text{Im}(\bar{\alpha})}{E_d \cos \phi}$ for $j = x, y$. Since $\bar{\alpha} \simeq iE_d \cos(\phi) [\Delta + i\kappa/2]^{-1}$ we then readily find:

$$g_{xy} \simeq g_x g_y \left[\frac{2\Delta \cot^2 \phi}{\Delta^2 + \frac{\kappa^2}{4}} \right], \quad g_{jz} \simeq g_j g_z \left[\frac{\kappa}{\Delta^2 + \frac{\kappa^2}{4}} \right] \quad (7)$$

Thus depending on the positioning, Δ or κ , the direct couplings contribution can be similar or exceed the cavity mediated coupling.

In Fig. 1(c) we compare analytical, closed form PSDs we obtained with 3D QLT and Eq. (4), with direct solutions of the nonlinear Langevin equations of motion, using the tweezer and cavity potential functions. In the latter, the g_j and g_{jk} are not parameters but rather simply emergent properties in the limit of low-amplitude displacements. The symmetrised analytical quantum spectra show excellent agreement with numerics in both quantum regimes as well as thermal (higher pressure regimes) provided the latter are cooled enough so that nonlinearities do not generate additional peaks in the optical spectra [15]. Furthermore, Fig. 1(c) also demonstrates the importance of the previously neglected g_{kj} terms: in particular, leading to double peaked structures ($x - y$ hybridisation) for $\phi \simeq 0$ where cavity mediated coupling $g_x g_y \simeq 0$ terms are negligible, as well as $\phi \rightarrow \pi/2$, where $g_{xy} \rightarrow 0$, but the cavity mediated coupling from $g_x g_y$ are strong.

However the $\phi = \pi/4$ case is the most interesting and represents a key finding: here the x - y hybridisation almost fully vanishes. Although both direct and indirect contributions are strong they interfere destructively. We can show that $i\eta^{(0)}(\omega) \rightarrow \frac{-2\Delta}{(\kappa/2)^2 + \Delta^2}$ if $-\Delta \gg \omega$ (and we are interested primarily in the region $\omega \sim \omega_j$). Thus for large $-\Delta$, using Eqs. (5) and (7), we can readily show

$$\mathcal{G}_{xy}^{3D}(\omega) \simeq g_x g_y \left[\frac{-2\Delta}{\Delta^2 + (\kappa/2)^2} \right] [1 - \cot^2 \phi], \quad (8)$$

and the x, y coupling $\mathcal{G}_{xy}^{3D}(\omega)$ thus vanishes.

We note $\phi \simeq \pi/4$, does not exactly correspond to $kx_0^{(c)} = k\lambda/8$, as there is an additional disturbance from co-trapping. Double structures are seen in the experimental x traces (see Fig. 3(c) of [21]), directly detected via scattered light, which we tentatively attribute to hybridisation even for a particle placed $\lambda/8$ from the antinode. The situation for the $\mathcal{G}_{jz}^{3D}(\omega)$ couplings is different as the z coupling is of the (non-standard for optomechanics) form $g_z i(\hat{a}^\dagger - \hat{a})\hat{z}$. The cancellation of z is partial, but nevertheless, all 3D couplings are attenuated for $-\Delta \gg \omega_j, \kappa$ (see [24] for details). Mixing with z is weaker as typically, $\omega_z \ll \omega_x, \omega_y$.

The transition from 3D to a near decoupled 1D regime seen above is further illustrated in Fig. 2 (left panels) where we have compared the PSDs obtained from 1D QLT (all $\mathcal{G}_{jk}^{3D} = 0$) with PSDs from the full 3D QLT. In

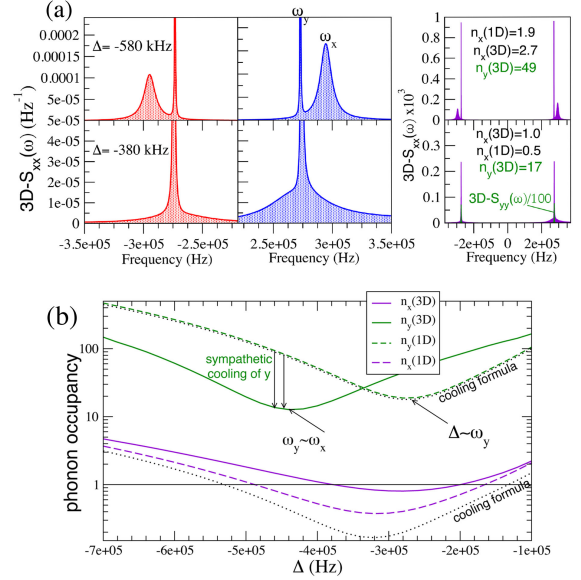


FIG. 3. Analysis of ground-state cooling experiments [23]. (a) Analytical $S_{xx}(\omega)$ PSDs reproduce well key experimental features of the blue and red sidebands. $\phi = \pi/2$ so we conclude there is pure cavity mediated coupling $\propto g_x g_y$ as $g_{xy} \simeq 0$. Also, $g_x \gg g_y$ since $\theta \simeq 0.47 - 0.49\pi$. (b) Shows 1D vs 3D phonon occupancies n_x, n_y . The results in (a) and (b) expose several remarkable features. (i) The sharp peak at $\omega \simeq \omega_y$, previously attributed to $S_{yy}(\omega)$, in fact arises mainly from hybridisation, hence the corresponding area should be considered in thermometry to validate measurements of $n_x < 1$. (ii) The narrow hybridisation peak shows very different asymmetry from the main broad $\omega \simeq \omega_x$ feature (see right panels of (a), showing both sidebands) so sideband asymmetry can only be measured from overall sideband area, not sideband heights. (iii) Surprisingly $n_y(3D)$ can be almost an order of magnitude lower than $n_y(1D)$, due to a novel optomechanical sympathetic cooling effect; the n_y minimum is displaced from the usual optomechanical cooling maximum at $\omega_y = -\Delta$. Dotted line plots in (b) results from the standard cooling formula of optomechanics that gives perfect agreement for 1D analytics, particularly for the weak coupled y mode. $R_0 = 71.5$, $\mathcal{F} = 73,000$, $P = 10^{-6}$ mbar. Detailed analysis is in [24].

Fig. 2 (right panels) we also look at the effect of ponderomotive quantum squeezing both for thermal regimes ($P = 10^{-7}$ mbar) as well as in the quantum back-action limit ($P = 0$). We see that as the x, y, z contributions interfere, the strong squeezing by one mode (z) can lower the noise imprecision floor for the other x, y modes (upper right panel).

In Fig. 3 we apply our theoretical analysis to the recent ground-state cooling experiments of [23] which are in the regime of $\phi = \pi/2$ (pure cavity-mediated coupling) and $\theta \simeq 0.47 - 0.49\pi$ (hence $g_x \gg g_y$). We reproduce the key experimental features but our analysis shows that the standard 1D analysis currently employed e.g. [23] may not yield accurate thermometry and that hybridisation-

related effects should be considered to establish whether the precise $n_x < 1$ threshold has been crossed (see [24] for details).

Conclusions.— We have shown that 3D optomechanical displacement sensing can be far from a trivial sum of PSDs associated to the \hat{x} , \hat{y} , and \hat{z} degrees of freedom. Although our work focusses on specifically on recent experiments on 3D cooling of levitated nanospheres, some of the conclusions are generic. We show one may be able to switch on and switch off some of the additional 3D effects and that these can give advantages in terms of exceeding usual quantum back action limited occupancies for a given coordinate. 3D optomechanics opens the way to new forms of force and displacement sensing, including sensing the direction as well as magnitude.

Acknowledgements.— We are extremely grateful to Uroš Delić for advice and for sharing with us details of the experimental data. We acknowledge support from EPSRC grant EP/N031105/1.

-
- [1] Warwick P. Bowen and Gerard J. Milburn. *Quantum Optomechanics*. CRC Press, 2015.
- [2] Markus Aspelmeyer, Tobias J. Kippenberg, and Florian Marquardt. Cavity optomechanics. *Rev. Mod. Phys.*, 86:1391–1452, Dec 2014.
- [3] B. P. Abbott et al. Observation of gravitational waves from a binary black hole merger. *Phys. Rev. Lett.*, 116:061102, Feb 2016.
- [4] James Millen, Tania S Monteiro, Robert Pettit, and Nick A. Vamivakas. Optomechanics with levitated particles. *arXiv:1907.08198*, 2019.
- [5] Zhang-Qi Yin, Andrew Geraci, and Tongcang Li. Optomechanics of levitated dielectric particles. *Int. J. Mod. Phys. B*, 27:1330018, 2013.
- [6] O. Romero-Isart, M.L. Juan, R. Quidant, and J.I. Cirac. Toward quantum superposition of living organisms. *New J. Phys.*, 12:033015, 2010.
- [7] D. E. Chang, C. A. Regal, S. B. Papp, D. J. Wilson, J. Ye, O. Painter, H. J. Kimble, and P. Zoller. Cavity opto-mechanics using an optically levitated nanosphere. *Proceedings of the National Academy of Sciences*, 107(3):1005–1010, 2010.
- [8] P. F. Barker and M. N. Shneider. Cavity cooling of an optically trapped nanoparticle. *Phys. Rev. A*, 81:023826, Feb 2010.
- [9] G. A. T. Pender, P. F. Barker, Florian Marquardt, J. Millen, and T. S. Monteiro. Optomechanical cooling of levitated spheres with doubly resonant fields. *Phys. Rev. A*, 85:021802, Feb 2012.
- [10] T. S. Monteiro, J. Millen, G. A T Pender, Florian Marquardt, D. Chang, and P. F. Barker. Dynamics of levitated nanospheres: Towards the strong coupling regime. *New Journal of Physics*, 15, 2013.
- [11] Nikolai Kiesel, Florian Blaser, Uroš Delić, David Grass, Rainer Kaltenbaek, and Markus Aspelmeyer. Cavity cooling of an optically levitated submicron particle. *Proceedings of the National Academy of Sciences*, 110(35):14180–14185, 2013.
- [12] Peter Asenbaum, Stefan Kuhn, Stefan Nimmrichter, Ugur Sezer, and Markus Arndt. Cavity cooling of free silicon nanoparticles in high vacuum. *Nature Communications*, 4:2743 EP –, Nov 2013. Article.
- [13] Pau Mestres, Johann Berthelot, Marko Spasenović, Jan Gieseler, Lukas Novotny, and Romain Quidant. Cooling and manipulation of a levitated nanoparticle with an optical fiber trap. *Applied Physics Letters*, 107(15):151102, 2015.
- [14] J. Millen, P. Z. G. Fonseca, T. Mavrogordatos, T. S. Monteiro, and P. F. Barker. Cavity cooling a single charged levitated nanosphere. *Phys. Rev. Lett.*, 114:123602, Mar 2015.
- [15] P. Z. G. Fonseca, E. B. Aranas, J. Millen, T. S. Monteiro, and P. F. Barker. Nonlinear dynamics and strong cavity cooling of levitated nanoparticles. *Phys. Rev. Lett.*, 117:173602, Oct 2016.
- [16] Lorenzo Magrini, Richard A. Norte, Ralf Riedinger, Igor Marinković, David Grass, Uroš Delić, Simon Gröblacher, Sungkun Hong, and Markus Aspelmeyer. Near-field coupling of a levitated nanoparticle to a photonic crystal cavity. *Optica*, 5(12):1597–1602, Dec 2018.
- [17] Vladan Vuletić, Hilton W Chan, and Adam T Black. Three-dimensional cavity doppler cooling and cavity sideband cooling by coherent scattering. *Physical Review A*, 64(3):033405, 2001.
- [18] David R Leibbrandt, Jaroslaw Labaziewicz, Vladan Vuletić, and Isaac L Chuang. Cavity sideband cooling of a single trapped ion. *Physical review letters*, 103(10):103001, 2009.
- [19] Mahdi Hosseini, Yiheng Duan, Kristin M Beck, Yu-Ting Chen, and Vladan Vuletić. Cavity cooling of many atoms. *Physical review letters*, 118(18):183601, 2017.
- [20] Dominik Windey, Carlos Gonzalez-Ballester, Patrick Maurer, Lukas Novotny, Oriol Romero-Isart, and René Reimann. Cavity-based 3d cooling of a levitated nanoparticle via coherent scattering. *Phys. Rev. Lett.*, 122:123601, Mar 2019.
- [21] Uroš Delić, Manuel Reisenbauer, David Grass, Nikolai Kiesel, Vladan Vuletić, and Markus Aspelmeyer. Cavity cooling of a levitated nanosphere by coherent scattering. *Phys. Rev. Lett.*, 122:123602, Mar 2019.
- [22] C. Gonzalez-Ballester, P. Maurer, D. Windey, L. Novotny, R. Reimann, and O. Romero-Isart. Theory for cavity cooling of levitated nanoparticles via coherent scattering: Master equation approach. *Phys. Rev. A*, 100:013805, Jul 2019.
- [23] Uroš Delić, Manuel Reisenbauer, Kahan Dare, David Grass, Vladan Vuletić, Nikolai Kiesel, and Markus Aspelmeyer. Motional quantum ground state of a levitated nanoparticle from room temperature. *arXiv:1911.04406*, 2019.
- [24] See supplementary information.
- [25] Jonathan Cripe, Nancy Aggarwal, Robert Lanza, Adam Libson, Robinjeet Singh, Paula Heu, David Follman, Garrett D. Cole, Nergis Mavalvala, and Thomas Corbitt. Measurement of quantum back action in the audio band at room temperature. *Nature*, 568:364, 2019.

SUPPLEMENTARY INFORMATION

Below we provide additional details of calculations in the main manuscript. In Section I we discuss further our analysis of the recent experiment reporting ground state cooling of levitated nanoparticles. In Section II we discuss suppression of hybridisation with the z motion. In Section III we provide details of the derivation of our 3D QLT (Quantum Linear Theory) of optomechanics expressions. Finally in Section IV we review details of the potentials in the coherent scattering system and their linearisation in order to infer the optomechanical couplings g_j as well as direct couplings g_{jk} for $j, k = x, y, z$.

S1. ANALYSIS OF GROUND-STATE COOLING EXPERIMENTS

In this section we discuss the recent experiment reported in [S1] which employs the 3D coherent scattering setup discussed in the main text. The experiment places the particle at the node ($\phi = \pi/2$) and is thus in regime of pure indirect, cavity-mediated coupling, which differs significantly from the regimes where direct/indirect pathways compete and cancel. Nonetheless, there are other novel and important features. The analysis confirms that the \hat{x} -motion is close to the ground state and identifies new effects in the \hat{x} and \hat{y} displacement spectra stemming from hybridisation between the \hat{x} to the \hat{y} motions. In particular, we find non-negligible corrections to phonon occupancies in both modes.

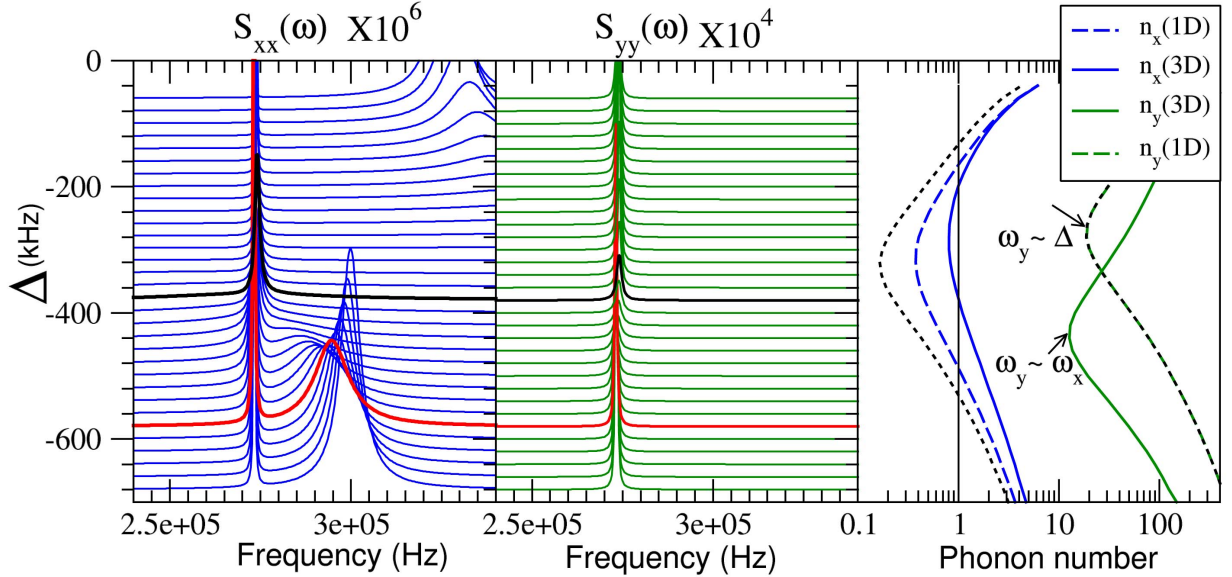


FIG. S1. Shows PSDs corresponding to \hat{x} and \hat{y} motions depicted using blue and green lines, respectively. The red (black) line correspond to the detuning $\Delta = -2\pi \times 580\text{kHz}$ ($\Delta = -2\pi \times 380\text{kHz}$) reported in [S1]. The PSDs are in units of Hz^{-1} but scaled as indicated for visibility. (Left panel) PSDs for \hat{x} -motion at different detunings Δ showing two notable features: (i) as the detuning approaches $-\Delta \sim \omega_x$, the x motion is optomechanically cooled to occupancies close to the ground state. (ii) as Δ is lowered, since $g_x \gg g_y$, the optical spring effect reduces ω_x , but leaves ω_y unperturbed, resulting in a frequency degeneracy $\omega_x \sim \omega_y$ that enhances hybridization effects and 3D heating/cooling channels. In particular, we note that S_{xx} , the \hat{x} PSD, contains a sharp peak at $\omega \simeq \omega_y$ due to the hybridisation. (Middle panel) \hat{y} -motion PSD $S_{yy}(\omega)$. The new 3D hybridisation affect cause significant cooling when the mechanical frequencies are degenerate (black line). (Right panel) Phonon occupancies n_x and n_y as a function of detuning, where 1D (3D) indicates a simplified one-dimensional (full three dimensional) analysis. We note that the phonon occupancy for the \hat{x} -motion indicates $n_x(3D) > n_x(1D)$. The \hat{y} -motion is cooled most effectively at the hybridization point, $\omega_y \sim \omega_x$. This latter effect is in contrast with the behaviour expected from a simplified 1D analysis, where cooling is most effective at $-\Delta = \omega_y$. Black dashed lines denote results from standard optomechanics cooling formula (see Eq.(S11)). We take $\theta = 0.47\pi$.

We have the following x - y hybridisation coupling strengths (see also Sec. S4 here):

$$\mathcal{G}_{xy}^{3D}(\omega) = \frac{i\mu_x(\omega)}{M_x(\omega)} \left[i\eta^{(0)}(\omega)g_xg_y + g_{xy} \right] \quad \text{and} \quad \mathcal{G}_{yx}^{3D}(\omega) = \frac{i\mu_y(\omega)}{M_y(\omega)} \left[i\eta^{(0)}(\omega)g_xg_y + g_{xy} \right]. \quad (\text{S1})$$

However, as the nanoparticle is located at a cavity node, $\phi = \pi/2$, they involve only the indirect cavity-field mediated coupling terms $\propto \eta^{(0)}(\omega)g_x g_y$ since the direct coupling coefficients vanish, i.e. $g_{xy} = 0$. Hence the x - y hybridisation couplings in the case of pure cavity-mediated interactions reduce to:

$$\mathcal{G}_{jk}^{3D} = -\frac{\mu_j \eta_0 g_j g_k}{1 + g_j^2 \mu_j \eta_0}, \quad (\text{S2})$$

where j, k denote the indices x and y . Interestingly, although in this configuration the cavity contains very few photons (only components at the Stokes/anti-Stokes frequencies), the indirect couplings still play a very important role.

In addition, the tweezer tilt-angle is set to values $\theta \approx \pi/2$, thus $g_y \ll g_x$, so one expects strong cooling exclusively along the x direction. However, the heterodyne detected PSDs showed prominent peaks at $\omega \simeq \omega_y$ (shifted by the reference oscillator) thus one infers that $g_y \neq 0$ so $\theta \neq \pi/2$. Allowing for an uncertainty in the tweezer tilt of a few degrees, we have thus assumed $\theta = (0.47 - 0.49)\pi$ to be consistent with the observations. For $\theta = 0.47 \times \pi$, we obtain $g_x \approx 2\pi \times 80\text{kHz}$ and $g_y \approx 2\pi \times 8\text{kHz}$, thus $g_x \approx 10g_y$.

A further detail of the observed data motivates a very small (10%) adjustment of the tweezer waist dimensions. Fig. S1 shows an optical-spring induced frequency degeneracy between the x and y modes at $\Delta \approx -400$ kHz, which is a feature of the experiments. In order to get agreement in the x, y frequencies as well as the frequency degeneracy, the tweezer waist values $w_x = 0.66\mu\text{m}$ and $w_y = 0.77\mu\text{m}$ in [S1] were reduced slightly to $w_x = 0.600\mu\text{m}$ and $w_y = 0.705\mu\text{m}$, which is consistent with inherent experimental uncertainties in the tweezer geometry.

Fig. S1 illustrates key features of the experimental regime in [S1], including the optical-spring induced degeneracy, the cooling dynamics, and the hybridisation. This is the scenario we now analyse. The z motion has a frequency $\omega_z \ll \omega_x, \omega_y$, and can thus be neglected in the simplified analysis below (but is included in the numerics). In this regime the x and y mechanical motions form a system of coupled equations, which in frequency space take the form:

$$\hat{x} = \tilde{D}_x^{1D} + \mathcal{G}_{xy}^{3D} \hat{y}, \quad (\text{S3})$$

$$\hat{y} = \tilde{D}_y^{1D} + \mathcal{G}_{yx}^{3D} \hat{x}. \quad (\text{S4})$$

The terms \tilde{D}_x^{1D} and \tilde{D}_y^{1D} denote the optical and mechanical noises which would be present already in a one-dimensional analysis, and the hybridization couplings \mathcal{G}_{jk}^{3D} are given in Eq. (S2).

A. Analysis of the y motion

Substituting Eq.(S3) into Eq.(S4) we find:

$$\hat{y} = \tilde{D}_y^{1D} + \mathcal{G}_{yx}^{3D} [\tilde{D}_x^{1D} + \mathcal{G}_{xy}^{3D} \hat{y}], \quad (\text{S5})$$

showing that the optomechanics introduces correlations between the x and y motions although the corresponding thermal noise fields are uncorrelated. As we are operating relatively far from the backaction limit, we neglect in the first instance the optical noises and hence the optically induced correlations between \tilde{D}_x^{1D} and \tilde{D}_y^{1D} . We note however that the above optomechanically induced correlations between the x and y modes are somewhat analogous to the well-studied correlations between optical and mechanical modes induced by optomechanical backaction.

As x is strongly cooled, we can in this case neglect the \tilde{D}_x^{1D} term. Hence,

$$\hat{y} \simeq (1 - \mathcal{G}_{yx}^{3D} \mathcal{G}_{xy}^{3D})^{-1} \tilde{D}_y^{1D} = \mathcal{N}^{-1}(\omega) \tilde{D}_y^{1D}, \quad (\text{S6})$$

and thus we arrive at an approximate expression for the PSD of \hat{y} :

$$S_{yy}^{3D} \simeq \frac{S_{yy}^{1D}}{|\mathcal{N}(\omega)|^2}. \quad (\text{S7})$$

Fig. S2 compares the above \mathcal{N} -rescaled PSD with the full analytical expressions, showing that the rescaling of the 1D sideband accurately accounts for the differences between the 3D and 1D PSDs including the relative heating and cooling.

In summary, around the frequency-degeneracy, there is strong (about factor 7) cooling of the y motion due to the x - y correlations and the backaction of y on x , i.e. the y mode is, via the cavity, coupled to x , and in turn the x mode, because of this cavity-mediated coupling, acquires a component correlated with the y thermal noises. We identify this as a new mechanism for ‘‘sympathetic cooling’’ of the y mode, due entirely to the strongly coupled (and strongly cooled) x mode.

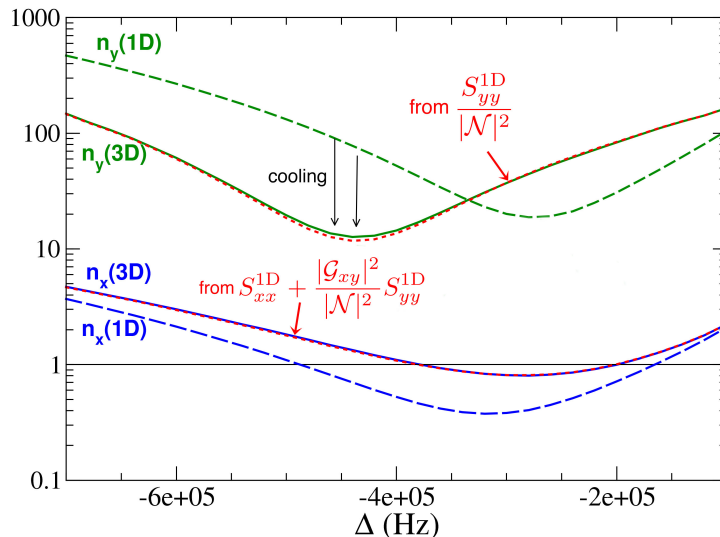


FIG. S2. Phonon occupancies n_x and n_y as a function of detuning showing that the 3D PSDs may be accurately estimated by a simple model that rescales the 1D PSDs (Eq.(S7) for y and Eq.(S9)); results showing the rescaled PSDs (in red) are in excellent agreement with the full 3D expressions.

B. Analysis of the x motion

The x motion can be analysed in similar manner, by substituting Eq.(S4) into Eq.(S3) which readily gives

$$\hat{x} = \mathcal{N}^{-1}(\omega) \left[\tilde{\mathcal{D}}_x^{1D} + \mathcal{G}_{xy}^{3D} \tilde{\mathcal{D}}_y^{1D} \right]. \quad (\text{S8})$$

Analogously, we find the PSD:

$$S_{xx}^{3D} \simeq S_{xx}^{1D} + \frac{|\mathcal{G}_{xy}^{3D}|^2}{|\mathcal{N}|^2} S_{yy}^{1D} \simeq S_{xx}^{1D} + |\mathcal{G}_{xy}^{3D}|^2 S_{yy}^{3D}, \quad (\text{S9})$$

where we have made the further approximation, based on inspection of the form of $\mathcal{N}(\omega)$, that $S_{xx}^{1D} \simeq S_{xx}^{1D} |\mathcal{N}|^{-2}$; in other words, the backaction of highly cooled x motion on the PSD of x , arising from its coupling to y , is relatively unimportant. The important difference between the S_{xx}^{3D} and S_{xx}^{1D} arises from the second term in Eq.(S9). This latter term is not an interference term, but an additive term, which always results in additional heating, and it provides the sharply peaked feature around $\omega \simeq \omega_y$.

This feature has previously been neglected, but its contribution to the sideband area should be included for accurate thermometry.

We note that the x sideband is strongly affected by the optomechanical spring effect. It is straightforward to adapt the usual analysis for this $x-y$ coupled case. One obtains the usual self-energy [S2] and (see Sec.IV for more details):

$$\Sigma_x \equiv \frac{g_x^2 \eta^{(0)}}{1 + g_y^2 \mu_y \eta^{(0)}}. \quad (\text{S10})$$

from whence we find the change of the damping, $\delta\Gamma$, and the shift of frequency that represents the optical spring effect, $\delta\omega$, using the following expressions [S2]:

$$\delta\Gamma_j = \frac{\text{Im}(\Sigma_j(\omega_j))}{\omega_j}, \quad \delta\omega_j = \frac{\text{Re}(\Sigma_j(\omega_j))}{2\omega_j}, \quad (\text{S11})$$

where ω_j denotes the mechanical frequency. Note the g_y^2 correction in the denominator of the self-energy; setting this to zero yields the standard 1D optomechanical cooling formula.

In Fig. S1 we compared phonon occupancies (black dashed lines, right panel) obtained in this way $n_x \simeq n_B \gamma_g / \Gamma_x$ where the thermal bath occupancy $n_B = kT / (\hbar\omega_x)$ for $T = 300\text{K}$. We note that the effect of this g_y^2 correction is small and the significant effects in heating of x arise rather from the hybridisation correction (the last term in Eq.(S9)).

C. Analysis of heterodyne-detected spectra: thermometry and sideband asymmetry

In [S1] the area under heterodyne-detected sidebands was evaluated to estimate phonon occupancies. However, the sharp peak at $\omega \sim \omega_y$ was excluded. A 3D analysis including hybridisation indicates this is likely to underestimate the area and hence the final phonon occupancy. It is interesting to estimate what proportion of the peak is due to y motion (and hence should be discounted when estimating n_x) and what proportion is due to hybridisation and thus contributes to the calculation of the energy in the x motion.

Heterodyne detection will detect y motion with amplitude $\propto g_y^2 |\eta^{(0)}(\omega)|^2 S_{yy}^{3D}(\omega)$, (where frequencies are shifted by the appropriate reference oscillator). We have shown that the 3D PSDs may be accurately estimated by a simple model employing rescaled PSDs (Eq.(S7) for y and Eq.(S9) for x). In turn, the hybridisation component in the heterodyne spectra is given by the second term in Eq.(S9) but its heterodyne detection amplitude scales with $g_x^2 |\eta^{(0)}(\omega)|^2$.

The $y : x$ component ratios may be estimated $1 : R$ where

$$R = \frac{g_x^2}{g_y^2} |\mathcal{G}_{xy}^{3D}(\omega \simeq \omega_y)|^2 \quad (\text{S12})$$

It is straightforward to plot the function $|\mathcal{G}_{xy}^{3D}(\omega)|^2$ and given $\frac{g_x}{g_y} \simeq 100$, we obtain $R = 1.8$ at $\Delta = -580$ kHz. In the hybridisation region $\Delta = -380 - 420$ kHz, we find $R \approx 3 - 5$ thus $\approx 70 - 90\%$ of the sharp peak is due to hybridisation and hence contributes to n_x thermometry. For the strongest cooling data, however at $\Delta = -300$ kHz, we find $R = 1.1$ thus in the strongest x cooling region, only half the $\omega \simeq \omega_y$ peak is due to hybridisation.

From the above analysis, we can see that the sharp peak to a good approximation carries the asymmetry of the y motion. If one eliminates asymmetry introduced by the cavity susceptibility function $|\eta^{(0)}(\omega)|^2$, the underlying asymmetry of the sharp $\omega \simeq \omega_y$ peak is $n_y(3D) + 1 : n_y(3D)$. In contrast, the asymmetry of the broad feature is closer to $n_x(1D) + 1 : n_x(1D)$.

This is in sharp contrast to the usual scenario in optomechanics where the red and blue sidebands have exactly the same shape but are simply rescaled by a factor $n/(n+1)$ where n is the appropriate occupancy. Here, the unusual hybridisation means that the full area of the sidebands including the y peak must be considered in order to estimate $n_x(3D)$ from sideband asymmetry.

S2. SUPPRESSION OF z HYBRIDISATION

In the main text we found that a remarkable transition from 3D to a near decoupled 1D regime occurs for $-\Delta \gg \omega_{x,y}$ and $\phi = \pi/4$, in between the 3D (direct coupled, $\phi \simeq 0$) and 3D (indirect, cavity mediated, $\phi \simeq \pi/2$) regimes. This results from the cancellation between the direct g_{xy} coupling and the cavity mediated $g_x g_y \eta^{(0)}$ terms; and underlying reason for this surprising near exact cancellation is that $g_{xy} \propto \text{Re}(\bar{\alpha})$ where $\bar{\alpha}$ is the mean cavity field, which follows the cavity resonance, that in turn determines the form of $\eta^{(0)}$.

However, the situation for the $\mathcal{G}_{jz}^{3D}(\omega)$ couplings is similar but more involved ($j \neq z$) so the destructive cancellation is less complete. A peculiarity of the system is that the z coupling is of the form $g_z i(\hat{a}^\dagger - \hat{a})\hat{z}$, i.e. the displacement couples to the *momentum* quadrature of the cavity. In this case, $\mathcal{G}_{jz}^{3D}(\omega) = \frac{i\mu_j(\omega)}{M_j(\omega)} [-i\eta^{(\pi/2)}(\omega)g_j g_z + g_{jz}]$, but $\mathcal{G}_{zj}^{3D}(\omega) = \frac{i\mu_z(\omega)}{M_z(\omega)} [i\eta^{(\pi/2)}(\omega)g_z g_j + g_{jz}]$. In other words, $\mathcal{G}_{jz}^{3D} \neq \mathcal{G}_{zj}^{3D}$ and both couplings cannot be suppressed simultaneously. In any case, using the equation from the main text:

$$g_{xy} \simeq g_x g_y \left[\frac{2\Delta \cot^2 \phi}{\Delta^2 + \frac{\kappa^2}{4}} \right], \quad g_{jz} \simeq g_j g_z \left[\frac{\kappa}{\Delta^2 + \frac{\kappa^2}{4}} \right] \quad (\text{S13})$$

and for large values of $-\Delta$ where $i\eta^{(\pi/2)} \rightarrow \frac{\kappa - 2i\omega}{\Delta^2 + (\kappa/2)^2}$, we find that $\mathcal{G}_{jz}^{3D}(\omega) \propto \frac{2g_j g_z i\omega}{\Delta^2 + (\kappa/2)^2}$ and $\mathcal{G}_{zj}^{3D}(\omega) \propto \frac{2g_j g_z [\kappa + i\omega]}{\Delta^2 + (\kappa/2)^2}$.

Thus even where there is destructive interference, only the real part of $\mathcal{G}_{jz}^{3D}(\omega)$ is fully cancelled. Nevertheless, all 3D couplings are attenuated for $-\Delta \gg \omega_j, \kappa$. Further, since fortunately since $\omega_z \ll \omega_{x,y}$, hybridisation between z and the other two modes is generally weaker than between x and y which are close in frequency. Thus it is possible to tune quite strongly into the decoupled 1D regime.

S3. QUANTUM LINEAR THEORY (QLT)

A. Standard optomechanics QLT

In this section we briefly review the framework of quantum linear theory (QLT) of optomechanics. Optically levitated systems [S3, S4] generally involve multiple optical and mechanical modes. Such multi-mode systems (N optical and M mechanical degrees of freedom) are typically described by the well-studied linearised Hamiltonian [S5]:

$$\hat{H} = \sum_{l=1}^{l=N} -\Delta_l \hat{a}_l^\dagger \hat{a}_l + \sum_{k=1}^{k=M} \omega_k \hat{b}_k^\dagger \hat{b}_k - \sum_{k,l} g_k^{(l)} (\hat{a}_l^\dagger + \hat{a}_l) (\hat{b}_k^\dagger + \hat{b}_k) \quad (\text{S14})$$

where \hat{a}_l (\hat{a}_l^\dagger) is the annihilation (creation) operator for optical mode l , and \hat{b}_k (\hat{b}_k^\dagger) for mechanical mode k . Δ_l is the detuning between the input laser and the cavity mode l , while ω_k is the natural frequency of the mechanical oscillator, and $g_k^{(l)}$ is the light-enhanced coupling strength between an optical mode and a mechanical mode. For simplicity, dissipation is characterised by a single optical damping rate, κ , and a single mechanical damping rate, Γ (though more complex scenarios, for example with multiple mirror losses, can be easily incorporated).

A set of $2(N + M)$ quantum Langevin equations of motion are obtained from Eq. (S14) by adding input noises. For example, for the single mode $N = M = 1$ case, where all $g_k^{(l)} \equiv g$, we have:

$$\begin{pmatrix} \dot{\hat{a}}(t) \\ \dot{\hat{a}}^\dagger(t) \\ \dot{\hat{b}}(t) \\ \dot{\hat{b}}^\dagger(t) \end{pmatrix} = \begin{pmatrix} i\Delta - \frac{\kappa}{2} & 0 & ig & ig \\ 0 & -i\Delta - \frac{\kappa}{2} & -ig & -ig \\ ig & ig & -i\omega - \frac{\Gamma}{2} & 0 \\ -ig & -ig & 0 & i\omega - \frac{\Gamma}{2} \end{pmatrix} \begin{pmatrix} \hat{a}(t) \\ \hat{a}^\dagger(t) \\ \hat{b}(t) \\ \hat{b}^\dagger(t) \end{pmatrix} + \begin{pmatrix} \sqrt{\kappa} \hat{a}_{\text{in}}(t) \\ \sqrt{\kappa} \hat{a}_{\text{in}}^\dagger(t) \\ \sqrt{\Gamma} \hat{b}_{\text{in}}(t) \\ \sqrt{\Gamma} \hat{b}_{\text{in}}^\dagger(t) \end{pmatrix}, \quad (\text{S15})$$

where \hat{a}_{in} (\hat{b}_{in}) is the optical (mechanical) input noise. The above equation even for arbitrary numbers of modes can be cast in matrix form:

$$\dot{\mathbf{c}}(t) = \mathbf{A}\mathbf{c}(t) + \mathbf{c}_{\text{in}}(t), \quad (\text{S16})$$

where the vector $\mathbf{c} = (\hat{a}_1 \hat{a}_1^\dagger \dots \hat{a}_N \hat{a}_N^\dagger \hat{b}_1 \hat{b}_1^\dagger \dots \hat{b}_M \hat{b}_M^\dagger)^\top$, the matrix \mathbf{A} contains the frequencies of the problem, and \mathbf{c}_{in} are Gaussian input noises (incoming quantum shot noise in the ideal case in the optical modes and thermal noise for the mechanical noises).

Multi-mode theoretical PSDs are efficiently computed using a the Linear Amplifier Model [S6]. For the LAM, the first step involves transforming the equations of motion into frequency space. The coupled equations are then manipulated analytically (or even numerically if unavoidable) to recast the matrix equation of the equations of motion in the form:

$$\mathbf{c}(\omega) = \mathbf{T}\mathbf{c}_{\text{in}}(\omega), \quad (\text{S17})$$

where $\mathbf{T}(\omega) = (-i\omega\mathbf{I} - \mathbf{A})^{-1}$ and \mathbf{I} is the identity. \mathbf{T} is a transformation matrix that characterises the transduction of the input noises into the mechanical and optical field fluctuations, somewhat analogous to the effect of a linear amplifier. The linear amplifier model is very powerful as one may in principle obtain the vector of all PSDs of all modes in one go:

$$S_{\mathbf{c}\mathbf{c}^\dagger}(\omega) = \mathbf{T}(\omega)\mathbf{N}\mathbf{T}^\dagger(\omega), \quad (\text{S18})$$

where

$$\langle \mathbf{c}_{\text{in}}(\omega) [\mathbf{c}_{\text{in}}(\omega)]^\dagger \rangle = \mathbf{N}, \quad (\text{S19})$$

and \mathbf{N} is a diagonal matrix of elements:

$$\mathbf{N} = \text{diag}(\gamma_1(\bar{n}_1 + 1) \quad \gamma_1\bar{n}_1 \quad \dots \quad \gamma_n(\bar{n}_n + 1) \quad \gamma_n\bar{n}_n). \quad (\text{S20})$$

The n_k represent the occupancy of the respective baths, thus $n_k = 0$ for quantum shot noise in the optical modes but $n_k \simeq kT/\hbar\omega_k$ for thermally occupied phonon modes. Typically, one can set $\gamma_k \equiv \kappa$ for optical modes and $\gamma_k \equiv \Gamma$ for the mechanical modes. For levitated systems there is no cryogenic cooling and $T = 300\text{K}$.

The solutions $\hat{a}_l(\omega)$ of the optical field denote here the intra-cavity field, while the actual detected cavity output field is then obtained using the input-output relation $\hat{a}_l^{\text{out}}(\omega) = \hat{a}_l^{\text{in}}(\omega) - \sqrt{\kappa}\hat{a}_l(\omega)$ for the respective optical mode.

B. 1D QLT with amplitude or phase optical coupling

In this section we consider one mechanical mode, \hat{b}_j , and one optical mode, \hat{a} , with two types of couplings: (i) $g_j(\hat{b}_j^\dagger + \hat{b}_j)(\hat{a}^\dagger + \hat{a})$ and (ii) $g_j(\hat{b}_j^\dagger + \hat{b}_j)i(\hat{a}^\dagger - \hat{a})$. The former case (i) is the usual optomechanical coupling between the mechanical mode and the amplitude quadrature of light which has been reviewed in Sec. S3 A. To obtain the PSD one can restrict the general multi-mode result in Eq. (S18) to the case of one optical and one mechanical degree of freedom by setting $N = M = 1$. Alternatively, an explicit calculation of the PSD can be performed by following the steps from Eqs. (S17)-(S20). Specifically, from Eq. (S15) one first moves to the frequency space and solves for the displacement operator $\hat{q}(\omega) = \hat{b}(\omega) + \hat{b}^\dagger(\omega)$, i.e. the displacement operator is expressed in terms of noises $\hat{a}_{\text{in}}(\omega)$ and $\hat{b}_{\text{in}}(\omega)$. The PSD can then be readily obtained by evaluating the expectation value using Eqs. (S19) and (S20). The latter case (ii), where the mechanical mode is now coupled to the phase quadrature of light, can be analysed using analogous steps. Specifically, one first obtains the quantum Langevin equations with the modified coupling and then follows the steps in Eqs. (S17)-(S20).

For both cases (i) and (ii) we can write the displacement operator using the notation adopted in the main text:

$$\hat{q}_j(\omega) \equiv \tilde{\mathcal{D}}_j^{1D} = M_j^{-1} \left[\sqrt{\Gamma} \tilde{Q}_j^{\text{therm}} + i\sqrt{\kappa} g_j \mu_j \tilde{Q}_\Phi^{\text{in}} \right], \quad (\text{S21})$$

where we have the normalization factor

$$M_j(\omega) = 1 + g_j^2 \mu_j(\omega) \eta^{(\Phi)}(\omega), \quad (\text{S22})$$

the mechanical susceptibilities

$$\mu_j(\omega) = \chi(\omega, \omega_j, \Gamma) - \chi^*(-\omega, \omega_j, \Gamma), \quad (\text{S23})$$

the mechanical noise

$$\tilde{Q}_j^{\text{therm}}(\omega) = \chi(\omega, \omega_j, \Gamma) \hat{b}_j^{\text{in}}(\omega) + \chi^*(-\omega, \omega_j, \Gamma) \hat{b}_j^{\text{in}\dagger}(\omega), \quad (\text{S24})$$

the optical susceptibility

$$\eta^{(\Phi)}(\omega) = e^{-i\Phi} \chi(\omega, -\Delta, \kappa) - e^{i\Phi} \chi^*(-\omega, -\Delta, \kappa), \quad (\text{S25})$$

the optical noise

$$\tilde{Q}_\Phi^{\text{in}}(\omega) = e^{-i\Phi} \chi(\omega, -\Delta, \kappa) \hat{a}_{\text{in}}(\omega) + e^{i\Phi} \chi^*(-\omega, -\Delta, \kappa) \hat{a}_{\text{in}}^\dagger(\omega), \quad (\text{S26})$$

and we have defined

$$\chi(\omega, \omega_j, \Gamma) = \left[-i(\omega - \omega_j) + \frac{\Gamma}{2} \right]^{-1}. \quad (\text{S27})$$

The above are (almost) the standard expressions for the 1D quantum linear theory (QLT) of optomechanics. The only difference is that we specify an angle Φ for the optical noise, such that $\Phi = 0$ for standard optomechanical coupling, i.e. coordinates coupled to the amplitude quadrature of light, but $\Phi = \pi/2$ for the coordinates coupled to the phase quadrature of light (such as the z coordinate in the experiments in [S7]).

C. 3D QLT with amplitude and phase optical coupling

In this section we consider three mechanical degrees of freedom that are coupled to both the amplitude and phase quadratures of the optical degree of freedom. Specifically, we consider the interaction Hamiltonian given by:

$$\frac{\hat{V}_{\text{int}}}{\hbar} = - \sum_j g_{jY} \hat{q}_j \hat{Y} - \sum_j g_{jP} \hat{q}_j \hat{P} - \sum_{j < k} g_{jk} \hat{q}_j \hat{q}_k, \quad (\text{S28})$$

where $\hat{Y} = \hat{a}^\dagger + \hat{a}$ and $\hat{P} = i(\hat{a}^\dagger - \hat{a})$, and $\hat{q}_j = \hat{b}_j^\dagger + \hat{b}_j$ denotes the mechanical degrees of freedom $\hat{x}, \hat{y}, \hat{z}$. The starting point of the analysis are again the equations of motion written in frequency domain:

$$\hat{q}_j(\omega) = J_{jY}(\omega)\hat{Y}(\omega) + J_{jP}(\omega)\hat{P}(\omega) + \sum_{k \neq j} J_{jk}(\omega)\hat{q}_k(\omega) + \sqrt{\Gamma}\tilde{Q}_j^{\text{therm}}(\omega), \quad (\text{S29})$$

$$\hat{Y}(\omega) = \sum_j J_{Yj}(\omega)\hat{q}_j(\omega) + \sqrt{\kappa}\tilde{Y}_{\text{in}}(\omega), \quad (\text{S30})$$

$$\hat{P}(\omega) = \sum_j J_{Pj}(\omega)\hat{q}_j(\omega) + \sqrt{\kappa}\tilde{P}_{\text{in}}(\omega), \quad (\text{S31})$$

where $J_{jk}(\omega) = ig_{jk}\mu_j(\omega)$ (for $j = x, y, z$, and $k = x, y, z, Y, P$), $J_{Yj}(\omega) = i(\tilde{g}_j\chi(\omega, -\Delta, \kappa) - \tilde{g}_j^*\chi^*(-\omega, -\Delta, \kappa))$, $J_{Pj}(\omega) = (\tilde{g}_j\chi(\omega, -\Delta, \kappa) + \tilde{g}_j^*\chi^*(-\omega, -\Delta, \kappa))$, and we have defined the complex-valued couplings $\tilde{g}_j = g_{jY} + ig_{jP}$. Note that in the main text, where we discuss a special case, we use the more common notation of real-valued couplings: $g_x \equiv g_{xY}$, and $g_y \equiv g_{yY}$, and $g_z \equiv g_{zP}$. The input noises are given by

$$\tilde{Q}_j^{\text{therm}}(\omega) = \chi^*(-\omega, \omega_j, \Gamma)b_j^{\text{in}\dagger}(\omega) + \chi(\omega, \omega_j, \Gamma)b_j^{\text{in}}(\omega), \quad (\text{S32})$$

$$\tilde{Y}_{\text{in}}(\omega) = \chi^*(-\omega, -\Delta, \kappa)a_{\text{in}}^\dagger(\omega) + \chi(\omega, -\Delta, \kappa)a_{\text{in}}(\omega), \quad (\text{S33})$$

$$\tilde{P}_{\text{in}}(\omega) = i(\chi^*(-\omega, -\Delta, \kappa)a_{\text{in}}^\dagger(\omega) - \chi(\omega, -\Delta, \kappa)a_{\text{in}}(\omega)), \quad (\text{S34})$$

where $\tilde{Q}_j^{\text{therm}}(\omega)$ denotes the mechanical noises $\tilde{X}^{\text{therm}}(\omega)$, $\tilde{Y}^{\text{therm}}(\omega)$, $\tilde{Z}^{\text{therm}}(\omega)$.

It is instructive to separate the contributions to the spectra of $\hat{q}_j(\omega)$ into two categories: one that contains the terms of a 1D approximation and one that contains additional terms arising in a realistic 3D problem. Specifically, using Eqs. (S30) and (S31) we can rewrite Eq. (S29) as:

$$\hat{q}_j(\omega) = \tilde{D}_j^{1D} + \sum_{k \neq j} \mathcal{G}_{jk}^{3D}(\omega)\hat{q}_k(\omega), \quad (\text{S35})$$

where \tilde{D}_j^{1D} is the displacement noise already present in 1D problems, and \mathcal{G}_{jk}^{3D} are new 3D couplings. In the main text we made the low order approximation $\hat{q}_k(\omega) \rightarrow \tilde{D}_k^{1D}$ to allow a simple analysis.

For example, for the special case of 3D coherent scattering discussed in the main text we find (see Sec. S4 for more details):

$$\mathcal{G}_{jk}^{3D}(\omega) = \frac{i\mu_j(\omega)}{M_j(\omega)} \left[i\eta^{(0)}(\omega)g_jg_k + g_{jk} \right], \quad (\text{S36})$$

$$\mathcal{G}_{jz}^{3D}(\omega) = \frac{i\mu_j(\omega)}{M_j(\omega)} \left[-i\eta^{(\pi/2)}(\omega)g_jg_z + g_{jz} \right], \quad (\text{S37})$$

$$\mathcal{G}_{zj}^{3D}(\omega) = \frac{i\mu_z(\omega)}{M_z(\omega)} \left[i\eta^{(\pi/2)}(\omega)g_zg_j + g_{zj} \right], \quad (\text{S38})$$

where in Eqs. (S36)-(S38) the indices j, k denote x or y .

We now continue with the general analysis. For numerical accuracy, we here give the exact expressions for the displacements in terms of noises. Specifically, starting from Eqs. (S29)-(S31) we eventually find:

$$\hat{q}_j(\omega) = A_j(\omega)\tilde{Y}_{\text{in}}(\omega) + B_j(\omega)\tilde{P}_{\text{in}}(\omega) + C_j(\omega)\hat{X}^{\text{therm}}(\omega) + D_j(\omega)\tilde{Y}^{\text{therm}}(\omega) + D_j(\omega)\tilde{Z}^{\text{therm}}(\omega), \quad (\text{S39})$$

where j denotes one of the mechanical motions,

$$A_j = N(\xi_{jx}\beta_{xY} + \xi_{jy}\beta_{yY} + \xi_{jz}\beta_{zY}), \quad (\text{S40})$$

$$B_j = N(\xi_{jx}\beta_{xP} + \xi_{jy}\beta_{yP} + \xi_{jz}\beta_{zP}), \quad (\text{S41})$$

$$C_j = N\xi_{jx}\beta_{xx}, \quad (\text{S42})$$

$$D_j = N\xi_{jy}\beta_{yy}, \quad (\text{S43})$$

$$E_j = N\xi_{jz}\beta_{zz}, \quad (\text{S44})$$

where $\beta_{jY} = N_j J_{jY}$, $\beta_{jP} = N_j J_{jP}$, $\beta_{jj} = N_j$, $N_j = (1 - J_{jY} J_{Yj} - J_{jP} J_{Pj})^{-1}$. We have defined the coefficients $\xi_{jj} = 1 - \frac{1}{2} R_{kl} R_{lk}$ (with $l, k \neq j$ and $k \neq l$), $\xi_{jk} = R_{jk} + R_{jl} R_{lk}$ (with $j \neq k$, $l \neq k$, and $l \neq j$), and $R_{jk} = N_j (J_{jY} J_{Yk} + J_{jP} J_{Pk} + J_{jk})$. The overall normalization is given by $N = (1 - \frac{1}{2} \sum R_{kl} R_{lk} - \frac{1}{3} \sum R_{kl} R_{lj} R_{jk})^{-1}$ (with $l \neq k, j \neq k$, and $l \neq j$). The PSDs can be readily obtained from Eq. (S39) using the methods discussed in Sec. S3A.

D. Self-energy, optical spring, and damping

In this section we obtain the analytical expressions for the self-energy, relevant to the experiments of [S1] that couple x and y (but not significantly z). We obtain also the resulting optical spring and damping formulae. We start from the coupled equations:

$$\hat{x} = J_{xy} \hat{Y} + \tilde{Q}_x^{\text{therm}}, \quad (\text{S45})$$

$$\hat{y} = J_{yx} \hat{Y} + \tilde{Q}_y^{\text{therm}}, \quad (\text{S46})$$

$$\hat{Y} = J_{Yx} \hat{x} + J_{Yy} \hat{y} + \tilde{Y}_{\text{in}}. \quad (\text{S47})$$

We now focus on the x -motion, while the formulae for the y motion can be obtained by formally exchanging $x \longleftrightarrow y$ in the formulae. Specifically, we solve for \hat{x} to find:

$$\hat{x} = J_{xY} [1 - J_{Yy} J_{yY}]^{-1} (J_{Yx} \hat{x} + J_{Yy} \tilde{Q}_y^{\text{therm}} + \tilde{Y}_{\text{in}}) + \tilde{Q}_x^{\text{therm}}. \quad (\text{S48})$$

One can then extract the self-energy Σ_x , which is given by:

$$\mu_x \Sigma_x \equiv - \frac{J_{xY} J_{Yx}}{1 - J_{Yy} J_{yY}}. \quad (\text{S49})$$

We note that the numerator is the usual term $\propto g_x^2$ which arises already in the 1D analysis, while the denominator term $\propto g_y^2$ is a new effect which arises in the 3D analysis. In particular, considering the expressions for J_{xY} and J_{Yx} we find from Eq. (S49):

$$\Sigma_x \equiv \frac{g_x^2 \eta^{(0)}}{1 + g_y^2 \mu_y \eta^{(0)}}. \quad (\text{S50})$$

Finally, we can find the change of the damping, $\delta\Gamma$, and the shift of frequency, $\delta\omega$, using the following expressions [S2]:

$$\delta\Gamma_j = \frac{\text{Im}(\Sigma_j(\omega_j))}{\omega_j}, \quad \delta\omega_j = \frac{\text{Re}(\Sigma_j(\omega_j))}{2\omega_j}, \quad (\text{S51})$$

where ω_j denotes the mechanical frequency.

S4. 3D LEVITATED OPTOMECHANICS IN A CAVITY DRIVEN BY COHERENTLY SCATTERED TWEEZER LIGHT

We consider the 3D optomechanical system such as the coherent scattering cavity levitation introduced in [S7–S9]. As discussed below, some of the optomechanical coupling terms are of the form $i g_k (\hat{a}^\dagger - \hat{a})(\hat{b}_k^\dagger + \hat{b}_k)$, i.e. the mechanical motion can couple to the phase quadrature of the light, in addition to the more typical coupling to the amplitude quadrature, i.e. $g_k (\hat{a}^\dagger + \hat{a})(\hat{b}_k^\dagger + \hat{b}_k)$. Specifically, we will consider the case when the z motion has the former type, while x and y motions have the latter one.

In addition, for a truly 3D system, one allows also direct couplings between the mechanical modes, i.e. $g_{kk'} \hat{q}_k \hat{q}_{k'}$, where $k, k' \equiv x, y, z$. Direct couplings are not usually considered in optomechanics: although multi-mode systems are commonly studied (such as multiple vibration modes of membranes) coupling between mechanical modes is not usually of interest. However for the considered 3D optical levitation this is not only important, but the $g_{kk'}$ are closely correlated with the couplings g_k . Specifically, we will find $g_{kk'} \propto g_k g_{k'}$, which has important consequences for sensing.

In particular, in a cavity populated only by scattered light as in the recent 3D set-ups in levitated optomechanics, we need consider only a single light mode, but three mechanical modes including direct coupling:

$$\hat{H} = \hat{H}_0 - (\hat{a}^\dagger + \hat{a})[g_x(\hat{b}_x^\dagger + \hat{b}_x) + g_y(\hat{b}_y^\dagger + \hat{b}_y)] - i(\hat{a}^\dagger - \hat{a})g_z(\hat{b}_z^\dagger + \hat{b}_z) - \sum_k \sum_{j \neq k} g_{jk}(\hat{b}_k^\dagger + \hat{b}_k)(\hat{b}_j^\dagger + \hat{b}_j) \quad (\text{S52})$$

where $\hat{H}_0 = -\Delta \hat{a}^\dagger \hat{a} + \sum_{k=x,y,z} \omega_k \hat{b}_k^\dagger \hat{b}_k$ (see Sec. S3 C where we have developed a generic framework to solve such Hamiltonians within QLT). In order to extract the dynamical parameters, i.e. the frequencies ω_k , the optomechanical couplings g_k , and the direct couplings g_{kj} , we must first consider the physical tweezer and cavity potentials (Sec. S4 A), and then expand to quadratic order around an equilibrium position (Sec. S4 B).

A. 3D coherent scattering Hamiltonian

We consider the hybrid tweezer-cavity experiments introduced in [S7], which employed set-ups very similar to those in [S8, S9]. A nanoparticle is trapped at the focus of a tweezer field and interacts with light coherently scattered from the tweezer field into the (undriven) cavity.

The Hamiltonian describing the interaction between the nanoparticle and the combined fields of the tweezer and cavity is given by:

$$\hat{H} = -\frac{\alpha}{2} |\hat{\mathbf{E}}_{\text{cav}} + \hat{\mathbf{E}}_{\text{tw}}|^2, \quad (\text{S53})$$

where $\hat{\mathbf{E}}_{\text{cav}}$ ($\hat{\mathbf{E}}_{\text{tw}}$) denotes the cavity (tweezer) field, $\alpha = 3\epsilon_0 V_s \frac{\epsilon_R - 1}{\epsilon_R + 2}$ is the polarizability of the nanosphere, V_s is the volume of the nanosphere, ϵ_0 is the permittivity of free space, and ϵ_R is the relative dielectric permittivity.

We assume a coherent Gaussian tweezer field and replace the modes with c-numbers to find:

$$\hat{\mathbf{E}}_{\text{tw}} = \frac{\epsilon_{tw}}{2} \frac{1}{\sqrt{1 + (\frac{z}{z_R})^2}} e^{-\frac{\hat{x}^2}{w_x^2}} e^{-\frac{\hat{y}^2}{w_y^2}} e^{ik\hat{z} + i\Phi(\hat{z})} e^{-i\omega_{tw}t} \mathbf{e}_y + \text{c.c.}, \quad (\text{S54})$$

where $\Phi(z) = -\arctan \frac{z}{z_R}$ is the Gouy phase, $z_R = \frac{\pi w_x w_y}{\lambda}$ is the Rayleigh range, w_x (w_y) are the beam waist along the x (y) axis, $\epsilon_{tw} = \sqrt{\frac{4P_{tw}}{w_x w_y \pi \epsilon_0 c}}$ is the amplitude of the electric field, c is the speed of light, P_{tw} is the laser power, ω_{tw} is the tweezer angular frequency, t is the time, and $\hat{\mathbf{r}} = (\hat{x}, \hat{y}, \hat{z})$ is the position of the nanoparticle. \mathbf{e}_j are the unit vectors: \mathbf{e}_z is aligned with the symmetry axis of the tweezer field and \mathbf{e}_y is aligned with the polarization of the tweezer field.

The cavity field is given by:

$$\hat{\mathbf{E}}_{\text{cav}} = \epsilon_c \cos(k(x_0^{(c)} + \hat{x}^{(c)})) \mathbf{e}_y^c [\hat{a} + \hat{a}^\dagger], \quad (\text{S55})$$

where $\epsilon_c = \sqrt{\frac{\hbar \omega_c}{2\epsilon_0 V_c}}$ is the amplitude at the center of the cavity, V_c is the cavity volume, ω_c is the cavity frequency, \hat{a} (\hat{a}^\dagger) is the annihilation (creation) operator, $x_0^{(c)}$ is an offset of the cavity coordinate system (centered at a cavity antinode) with respect to the tweezer coordinate system. The cavity x_c - y_c plane is rotated by an angle θ with respect to the tweezer x - y plane:

$$\begin{bmatrix} x_c \\ y_c \end{bmatrix} = \begin{bmatrix} \sin(\theta) & \cos(\theta) \\ -\cos(\theta) & \sin(\theta) \end{bmatrix} \begin{bmatrix} x \\ y \end{bmatrix}. \quad (\text{S56})$$

Note that for $\theta = 0$ the tweezer polarization (y -axis) becomes aligned with the cavity symmetry axis (x_c -axis). In particular, we have $\hat{x}^{(c)} = \sin(\theta)\hat{x} + \cos(\theta)\hat{y}$. Furthermore, we then have the following relation between the cavity and tweezer unit vectors

$$\mathbf{e}_y^c = [-\mathbf{e}_x \cos(\theta) + \mathbf{e}_y \sin(\theta)]. \quad (\text{S57})$$

We expand the Hamiltonian in Eq. (S53) exploiting Eqs. (S54), (S55), and (S57) to obtain three terms:

$$\hat{H} = -\frac{\alpha}{2}|\hat{\mathbf{E}}_{\text{tw}}|^2 - \frac{\alpha}{2}|\hat{\mathbf{E}}_{\text{cav}}|^2 - \frac{\alpha\sin(\theta)}{2}(\hat{\mathbf{E}}_{\text{cav}}^\dagger\hat{\mathbf{E}}_{\text{tw}} + \hat{\mathbf{E}}_{\text{cav}}\hat{\mathbf{E}}_{\text{tw}}^\dagger), \quad (\text{S58})$$

where the terms on the right hand-side are the tweezer term, the cavity term, and the tweezer-cavity interaction term (from left to right). The first (tweezer field) term dominates the trapping and primarily sets the three mechanical frequencies ω_x , ω_y , and ω_z . The second term provides a (typically) small correction to the frequencies and is included only for numerical precision. The third term, which we will denote as \hat{V}_{int} , is the most interesting and novel form of optomechanical interaction. As discussed in [S7, S9], time-dependencies in this term are eliminated through rotating frame approximations leaving an effective optomechanical Hamiltonian:

$$\frac{\hat{V}_{\text{int}}}{\hbar} = -E_d\cos(\phi + k(\hat{x}\sin\theta + \hat{y}\cos\theta)) \left[\hat{a}e^{-i(k\hat{z} + \Phi(\hat{z}))} + \hat{a}^\dagger e^{+i(k\hat{z} + \Phi(\hat{z}))} \right], \quad (\text{S59})$$

where $E_d = \frac{\alpha\epsilon_c\epsilon_{\text{tw}}\sin\theta}{2\hbar}$, $\phi = kx_0^{(c)}$ represents the effect of the shift between the origin of the cavity and tweezer. The experiments allow positioning of $x_0^{(c)}$ with an accuracy of ~ 8 nm for $\lambda = 1064$ nm. In first approximation one can neglect the Gouy phase Φ . Linearisation of the above Hamiltonian to quadratic order yields the 3D optomechanical couplings.

B. Quadratic Hamiltonian: unified form

We expand the Hamiltonian in Eq. (S59) around an equilibrium point $(x_0, y_0, z_0, \bar{\alpha})^\top$ by making the substitution $(x, y, z, a)^\top \rightarrow (x_0, y_0, z_0, \bar{\alpha})^\top + (x, y, z, a)^\top$, where $(x, y, z, a)^\top$ on the right hand-side denotes small fluctuations.

To a first approximation, x_0, y_0, z_0 represents the origin of the strong tweezer trap; however, as investigated in [S9], when the cavity is strongly populated, this must be corrected with further small offsets $\delta x_0, \delta y_0, \delta z_0$. These emerge naturally from numerical simulations and can also be well estimated through the linearisation analysis. The mean cavity photon occupancy number $n = |\bar{\alpha}|^2$ may also need to be corrected from the approximate form [S7] $\bar{\alpha} = -iE_d\cos(\phi)/(i\Delta - \kappa/2)$ to allow for the fact that $\phi \simeq kx_0^{(c)} + \delta x_0\cos\theta + \delta y_0\sin\theta$ must include the additional corrections to $x_0^{(c)}$.

A unique feature of these new levitated set-ups is that the optomechanical coupling can be via the momentum quadrature. In the calculation in [S7–S9] this affected only the z coordinate. However, we note that if there are significant offsets in the fields or misalignment of the cavity and tweezer axes, in general, one might wish to consider both amplitude and momentum couplings to all mechanical modes so here we introduce a unified notation.

It is convenient to introduce the notation $\hat{Y} = \hat{a}^\dagger + \hat{a}$, and $\hat{P} = i(\hat{a}^\dagger - \hat{a})$ for the optical field. We also similarly use $\hat{x} = x_{\text{zpf}}(\hat{b}_x^\dagger + \hat{b}_x)$, $\hat{y} = y_{\text{zpf}}(\hat{b}_y^\dagger + \hat{b}_y)$, $\hat{z} = z_{\text{zpf}}(\hat{b}_z^\dagger + \hat{b}_z)$, where zero-point fluctuation lengths are given by $x_{\text{zpf}} = \sqrt{\frac{\hbar}{2m\omega_x}}$, $y_{\text{zpf}} = \sqrt{\frac{\hbar}{2m\omega_y}}$, and $z_{\text{zpf}} = \sqrt{\frac{\hbar}{2m\omega_z}}$, and m is the mass of the levitated nanoparticle.

Redefining $\hat{x}/x_{\text{zpf}} \rightarrow \hat{x}$, $\hat{y}/y_{\text{zpf}} \rightarrow \hat{y}$, and $\hat{z}/z_{\text{zpf}} \rightarrow \hat{z}$ we write:

$$\frac{\hat{H}}{\hbar} = - \left[g_{xy}\hat{x}\hat{y} + g_{xz}\hat{x}\hat{z} + g_{yz}\hat{y}\hat{z} + (g_{xY}\hat{x} + g_{yY}\hat{y} + g_{zY}\hat{z})\hat{Y} + (g_{xP}\hat{x} + g_{yP}\hat{y} + g_{zP}\hat{z})\hat{P} \right], \quad (\text{S60})$$

where we have omitted the harmonic oscillator terms. We can also rewrite the optical quadratures in terms of the mode operator \hat{a} :

$$\frac{\hat{H}}{\hbar} = - \left[g_{xy}xy + g_{xz}z + g_{yz}yz + (\tilde{g}_x x + \tilde{g}_y y + \tilde{g}_z z)a^\dagger + (\tilde{g}_x^* x + \tilde{g}_y^* y + \tilde{g}_z^* z)a \right], \quad (\text{S61})$$

where we have introduced the complex-valued couplings $\tilde{g}_j = g_{jY} + ig_{jP}$ (see Sec. S3 C for the resolution of this general Hamiltonian within 3D QLT). However in the following we opt to use the more conventional notation introduced for the special case in Eq. (S52) where all the coupling constants are defined as real-valued. Specifically, from Eq. (S59) we find the following non-zero light-matter couplings:

$$g_x \equiv g_{xY} = -E_d k \sin(\theta) \sin(\phi) x_{zpf}, \quad (\text{S62})$$

$$g_y \equiv g_{yY} = -E_d k \cos(\theta) \sin(\phi) y_{zpf}, \quad (\text{S63})$$

$$g_z \equiv g_{zP} = E_d k \cos(\phi) z_{zpf}. \quad (\text{S64})$$

In addition we also have matter-matter couplings

$$g_{xy} = -E_d k^2 Y_0 \sin(\theta) \cos(\theta) \cos(\phi) x_{zpf} y_{zpf}, \quad (\text{S65})$$

$$g_{xz} = -E_d k^2 P_0 \sin(\theta) \sin(\phi) x_{zpf} z_{zpf}, \quad (\text{S66})$$

$$g_{yz} = -E_d k^2 P_0 \cos(\theta) \sin(\phi) y_{zpf} z_{zpf}. \quad (\text{S67})$$

The harmonic frequencies are given by

$$\omega_j = \sqrt{\frac{1}{m}(T_j + C_j + T_j^c)}, \quad (\text{S68})$$

where $T_x = \frac{\alpha \epsilon_{tw}^2}{w_x^2}$, $T_y = \frac{\alpha \epsilon_{tw}^2}{w_y^2}$, and $T_z = \frac{\alpha \epsilon_{tw}^2}{2z_R^2}$ are the typically dominant contributions arising from the tweezer trap. The corrections from the cavity are $C_x = 2\alpha \epsilon_c^2 k^2 n \sin^2(\theta) \cos(2\phi)$ and $C_y = 2\alpha \epsilon_c^2 k^2 n \cos^2(\theta) \cos(2\phi)$, and $C_z = 0$. The contributions arising from the coupling between the cavity and tweezer are $T_x^c = \frac{\hbar E_d}{w_x^2} (2 + k^2 w_x^2 \sin^2(\theta)) Y_0 \cos(\phi)$, $T_y^c = \frac{\hbar E_d}{w_y^2} (2 + k^2 w_y^2 \cos^2(\theta)) Y_0 \cos(\phi)$, and $T_z^c = \frac{\hbar E_d}{z_R^2} (1 + k^2 z_R^2) Y_0 \cos(\phi)$. We remark that corrections from C_j and T_j^c can in certain cases become important, e.g. when the cavity has a high photon occupancy, potentially even leading to nanoparticle loss. The cavity-tweezer interaction also changes the cavity detuning from Δ to $\Delta + \Delta_0$, where $\Delta_0 = \frac{\alpha \epsilon_c^2}{\hbar} \cos^2(\phi)$.

-
- [S1] Uroš Delić, Manuel Reisenbauer, Kahan Dare, David Grass, Vladan Vuletić, Nikolai Kiesel, and Markus Aspelmeyer. Motional quantum ground state of a levitated nanoparticle from room temperature. *arXiv:1911.04406*, 2019.
- [S2] Florian Marquardt, Joe P Chen, Aashish A Clerk, and SM Girvin. Quantum theory of cavity-assisted sideband cooling of mechanical motion. *Physical review letters*, 99(9):093902, 2007.
- [S3] James Millen and Andre Xuereb. Perspective on quantum thermodynamics. *New Journal of Physics*, 18(1):011002, 2016.
- [S4] E.B. Aranas, M Javed Akram, Daniel Malz, and T.M. Monteiro. Quantum noise spectra for periodically driven cavity optomechanics. *Phys.Rev.A*, 96:063836, 2017.
- [S5] Warwick P. Bowen and Gerard J. Milburn. *Quantum Optomechanics*. CRC Press, 2015.
- [S6] T Botter, D.W.C. Brooks, N Brahms, S Schreppler, and Dan M Stamper-Kurn. Linear amplifier model for optomechanical systems. *Phys. Rev. A*, 85:013812, 2012.
- [S7] Uroš Delić, Manuel Reisenbauer, David Grass, Nikolai Kiesel, Vladan Vuletić, and Markus Aspelmeyer. Cavity cooling of a levitated nanosphere by coherent scattering. *Phys. Rev. Lett.*, 122:123602, Mar 2019.
- [S8] Dominik Windey, Carlos Gonzalez-Ballester, Patrick Maurer, Lukas Novotny, Oriol Romero-Isart, and René Reimann. Cavity-based 3d cooling of a levitated nanoparticle via coherent scattering. *Phys. Rev. Lett.*, 122:123601, Mar 2019.
- [S9] C. Gonzalez-Ballester, P. Maurer, D. Windey, L. Novotny, R. Reimann, and O. Romero-Isart. Theory for cavity cooling of levitated nanoparticles via coherent scattering: Master equation approach. *Phys. Rev. A*, 100:013805, Jul 2019.